J Mater Sci (2008) 43:5031–5035
DOI 10.1007/s10853-008-2744-5

LETTER

Multi-phenomena simulation of electric field assisted sintering

Brandon McWilliams · Antonios Zavaliangos

Received: 20 March 2008 / Accepted: 19 May 2008 / Published online: 5 June 2008

Electric field assisted sintering technique (FAST) is a single step processing operation for producing bulk (near fully dense) materials from powders. The powder is placed in a conductive die and pressed with conductive punches under pressure while electric current is applied. This process differs from other powder processing techniques such as HIP and press and sinter operations where the powder or compact is heated externally in that the powder is heated directly as a result of internal Joule heating (for conductive powders) and/or by conduction from the die and punches. The overall result is much more efficient heating which allows heating rates of >1000 °C/min to be achieved [1]. These very high heating rates can lead to non-uniform distributions of electrical current and temperature fields. In conductive powders, Joule heating may be localized, causing the evolution of temperature within the powder to be highly dependent upon local properties and variations in density. Coupled with the fact that the powder is not pressed prior to sintering, a situation arises where the sample will be nearly insulating at the beginning of the process and transition to conductive upon densification [2]. This dramatic variation in properties can have a profound effect on the local temperature history and resulting final properties/performance of the part [3].

The complex nature of the electrical and thermal gradients present during the FAST process was first explored numerically by Zavaliangos et al. [4] using a finite element model. This work highlighted that the die surface and specimen are generally at different temperatures, which is a concern for process control. They showed the importance of contact resistances within the system on the distribution of current and temperature. These contact resistances were shown to be dependent on applied pressure [5]. A similar modeling approach in conjunction with experiments was presented in [6] to evaluate the effect of material properties on the local temperature field distribution in two different ceramics. Other finite element modeling results [7] have shown that tooling geometry also has a significant impact on the resulting electrical and thermal field distributions.

Despite the progress made to date, prior work has been aimed at studying thermal-electric phenomena without any consideration of the evolution of density which in turn may affect the thermal and electrical properties. Zhang [2] made an attempt to incorporate punch motion during FAST. The sintering of a cylinder was approximated by a sequence of different finite element discretizations assuming that density was uniform in the specimen. The variation of height was obtained from experimental data. This approach does not work when significant density variation is present in the sample. Thus, a need exists to model the coupling of the thermal-electric and sintering phenomena. A fully coupled thermal-electric-sintering model is required to account for evolution of material properties due to densification as well as the displacement of punches. A fully coupled model of the FAST process will be useful in process optimization for materials sensitive to local variations in temperature field such as nanopowders, and in optimization for scale-up efforts to produce larger/more complex parts. The work presented in this paper focuses on model development and a numerical case study of the sintering of a rectangular compact with an initial density variation under the application of an applied electric field.

To this end, a two-part finite element approach was utilized to create a fully coupled model that incorporates thermal, electrical, and sintering phenomena. The two

B. McWilliams (✉) · A. Zavaliangos
Department of Materials Science and Engineering,
Drexel University, Philadelphia, PA 19104, USA
e-mail: brandon.mcwilliams4@arl.army.mil

modules consist of a thermal-electric simulation and a sintering (thermal-displacement) simulation. The temperature history resulting from an external current applied over a short time period, Δt, is calculated by a coupled thermal-electric simulation which considers a fixed specimen geometry. This is used as an input to the sintering simulation which tracks the local relative density and produces an estimate of the shape and volume evolution of the specimen during the same time period Δt. The updated mesh is fed to the thermoelectric simulation and the process is iterated. In addition, stresses at the end of each sintering iteration are stored to maintain continuity over time. A schematic of the algorithm is shown in Fig. 1. All finite element simulations were run using the commercial package ABAQUS.

A two-dimensional rectangle of 10 × 20 mm is considered in this set of simulations. A study of the effect of thermal diffusivity on the overall densification behavior was carried out. Four case studies of different material configurations were run to evaluate the proposed algorithm. In all cases the sintered body consists of two layers of different initial relative density ($RD_{0L} = 0.59$ and $RD_{0H} = 0.69$) along the shorter dimension of the specimen with a ratio of thicknesses: $t_L/t_H = 4$. The electric current is applied such that the two layers are in either series or parallel configuration (stacked normal or parallel to the direction of applied current). The current is applied directly to the corresponding surface nodes of the compact which maintains the electrical input even in the event of sample distortion due to sintering in the absence of applied pressure (i.e., there is no loss of contact with an electrode). The two configurations were repeated with the thermal diffusivity decreased by one order of magnitude (initial density

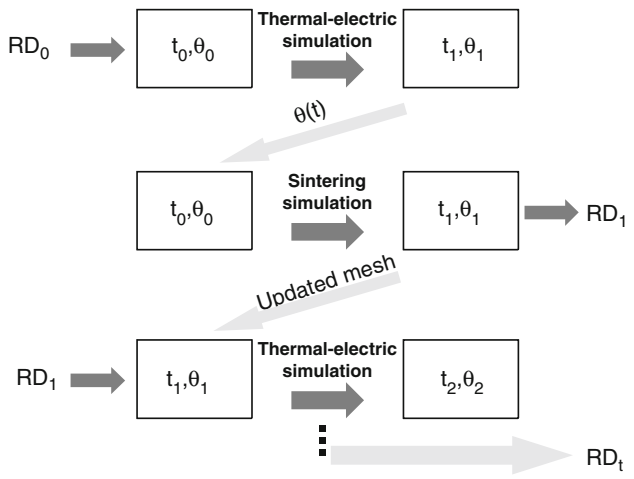

Fig. 1 Schematic of simulation algorithm. During a thermoelectric step the density is fixed. For an adequately small time increment this algorithm is equivalent to a fully coupled simulation that takes into account all three phenomena

configurations can be seen in Fig. 2). Such density and material gradients are possible by design, or can result from die filling and pressing operations.

The thermal-electric simulations are fully coupled, with the temperature history coming solely from heat generation due to Joule heating effects. The difference in specific heat between the two sets of samples necessitates an adjustment to the current input to achieve the same heating rate for all samples. The initial current input was 11 kA for the samples i and ii (higher thermal diffusivity), and 27 kA for samples iii and iv (lower thermal diffusivity) after which the current was increased in a stepwise manner at a rate of 300 A/min. This generated a heating rate of ~105 °C/min for all samples. The simulations were stopped when the material reached full density. The material properties vary with temperature and relative density. The temperature dependence of the material properties has been discussed in [7, 8], while the density dependence of thermal and electrical conductivity was assumed to be given by:

$$\frac{k_{\text{eff}}}{k_s} = \exp(7\rho - 7), \frac{\sigma_{\text{eff}}}{\sigma_s} = \exp(7\rho - 7) \quad (1)$$

where ρ is the relative density, k and σ are the thermal and electrical conductivity with subscripts s and eff indicating the fully dense and the effective values, respectively. Material properties were assumed of a model conductive material similar to tungsten carbide cobalt (WC-Co) with the thermal conductivity roughly doubled. It is emphasized that the goal of this work is process understanding rather than direct predictions of experimental results. The fully dense (14.4 g/cm^{-3}) thermal and electrical conductivity were taken to be 162 Wm^{-1} K^{-1} and 1.93 × 10^7 Sm^{-1}, respectively. The heat capacity of the fully dense material is 200 J kg^{-1} K^{-1}.

To achieve lower thermal diffusivity for samples iii and iv, the thermal conductivity was decreased by a factor of 2, while the overall heat capacity was increased by a factor of 5.

The constitutive equations for sintering are based on the work of Bouvard [9, 10]. In this phenomenological model, the densification kinetics

$$\dot{\varepsilon}_s = \Omega(T)(\rho_\infty(T) - \rho)^n \quad (2)$$

are fitted to experimental data obtained from a single staircase sintering cycle. In this equation, $\rho_\infty(T)$ is the maximum relative density that can be reached at a given isothermal sintering step, and $\Omega(T)$ and n are fitting parameters as a function of temperature. This constitutive model is implemented in ABAQUS via a creep user subroutine. Stresses calculated from the analysis are input to the subroutine and used with the constitutive model to determine the increment in creep strain. The volumetric creep strain is used to update the relative density at the end

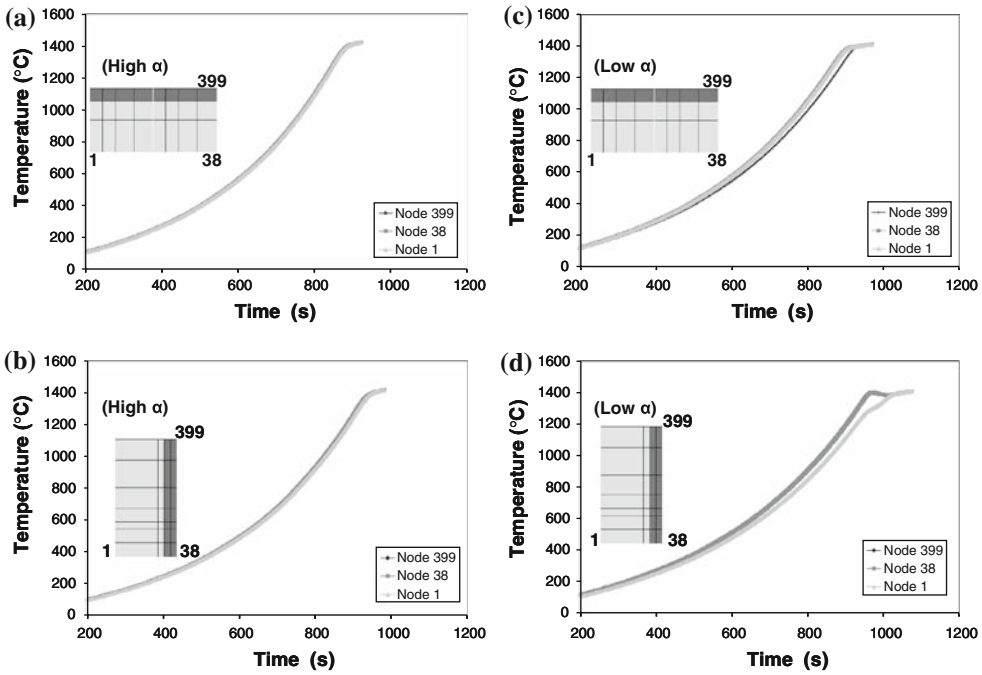

Fig. 2 Temperature histories of selected points for the four examples used in this study. (**a**) Series sample with baseline thermal diffusivity; (**b**) parallel sample with baseline thermal diffusivity; (**c**) series sample with reduced thermal diffusivity; and (**d**) parallel sample with reduced thermal diffusivity. Points for histories are identified in the inset mesh

of each increment. The present case study considers only free sintering, i.e., the compact is not constrained in a die or under pressure. The model presented here was implemented in ABAQUS in a way that can take into account elastic properties as functions of relative density. The value of Young's modulus determines the maximum stable time increment in the simulation. For the free sintering problem examined here, the elastic strains involved are very small (<0.01%). For efficiency purposes we chose to implement fixed elastic properties for all densities. For this specific problem results were rather insensitive to the value of modulus with ±1 order of magnitude of the values used. Finally it was established that alternation between sintering and thermoelectric simulations every 5 s of process time provided adequate discretization of the problem. The total sintering strain varied by less than 0.5% when 5 and 10 s intervals were compared. The values used for the Young's modulus and Poisson's ratio were 5 GPa and 0.3, respectively.

For both cases of thermal diffusivity, the current density was uniform throughout the sample in the series arrangement, whereas in the parallel case more current flows through the region of initially higher density due to its lower resistance. This difference in current path leads to differential heating and densification results depending on the thermal diffusivity. The simulation predictions for the temperature histories of the sintering cycle are presented in Fig. 2. In the series cases, more heat is generated in the lower density layer where the resistance is higher, whereas in the parallel cases the high-density layer heats faster. In the simulations with higher thermal diffusivity, preferential heat generation in a layer is quickly dissipated to the other layer, and the temperature throughout the sample remains mostly uniform (maximum $\Delta T < 13$ °C) for both arrangements throughout the run. While both layers densify at approximately the same rate, there is distortion of the compact's geometry (Fig. 3) due to the differential shrinkage involved in going to full density from different initial densities.

On the other hand, the densification kinetics of the lower thermal diffusivity samples is governed by the heat generation of each layer. Therefore the temperature gradient within the sample is much higher and a maximum ΔT of 105 °C develops in the parallel case and a ΔT of 75 °C in the series arrangement. In the parallel sample, the temperature is higher in the high-density layer since heating is dominated by high current density. In the series example, heating is dominated by the resistance of the material, and the higher temperature is present in the low-density layer. This effect is readily observed in the resulting densification of the sample (Fig. 3a and c). Heat flux from the higher temperature low-density layer to the low temperature high-density layer results in a transient cooler band and lower density region in the middle of the specimen. The onset of densification is also sooner and the overall sintering process is shorter for the series arrangement since heating is taking place in a larger volume (the low density layer). In the series case, the low-density material sinters to full density before the high-density layer begins to densify. This differential densification results in distortion of the compact until the higher density layer begins to densify and "catches up" (Fig. 3c) at which time the distortion

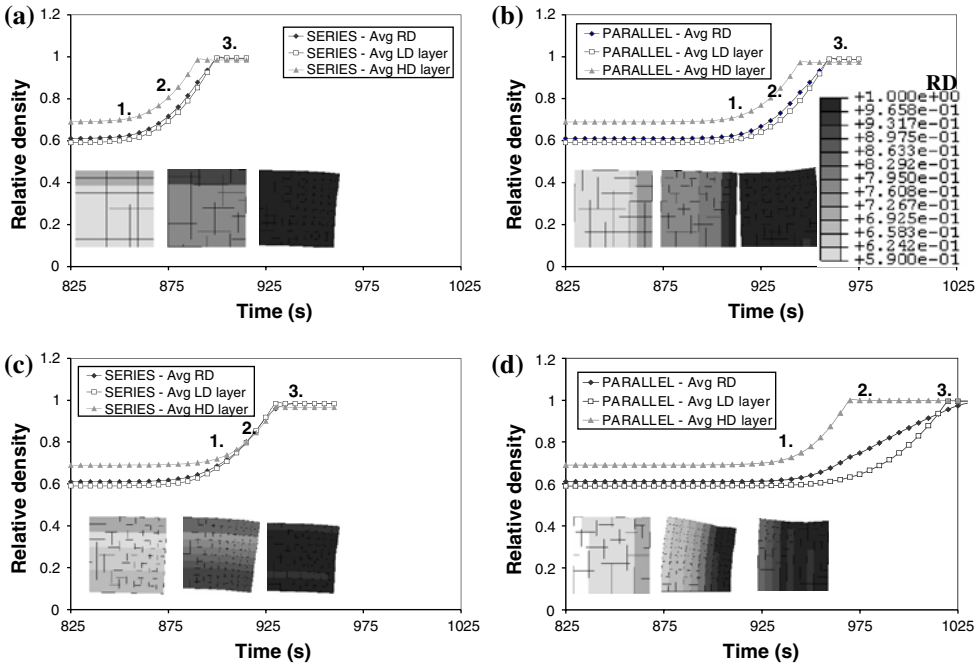

Fig. 3 Relative density histories for the four examples used in this study. (**a**, **b**) Series and parallel samples with baseline thermal diffusivity; (**c**, **d**) corresponding samples with reduced thermal diffusivity. Relative density contours are shown (inset) for points indicated and represent half the 2D model

decreases but remains present even when all material is fully dense due to the difference in the initial densities. The parallel case follows a different densification path. In this case, the high-density layer heats and densifies completely before the lower initial density layer sinters at all. Since the high-density layer is relatively thin (20% of the compact), a reversal of the distortion occurs as sintering proceeds in the lower initial density layer (Fig. 3d). In both cases, the temperature field homogenizes (Fig. 2c, d) as the material densifies and the resistances of each layer decrease and approach that of the fully dense material.

When the heat conduction length scale is of the same order as the length scale of the higher density regime in the parallel series arrangement, it is conceivable that a self-accelerating heating situation may develop. In other words, heat in the high-density region, which densifies quicker the material, cannot be dissipated and accelerated sintering by further increasing the local density of the material. Raichenko [11] discusses experimental observations of current localization in conductive powders along paths of least resistance and resultant heat generation which can result in the local heat to be high enough to melt the conductive material and result in "channels" of sintered material leaving the rest of the specimen poorly sintered.

The fully coupled thermal-electric-sintering model developed for the simulation of electric field activated sintering processes presented in this work successfully accounts for sintering and can predict distortions caused by non-uniform initial densities and most importantly the evolution of material properties of a conductive material during the course of densification. It was shown that variances in local densities and material properties (thermal diffusivity) can dramatically affect the overall sintering behavior of a sample. This has severe implications for parts with inhomogeneous initial density fields, as samples with the same average final density may have undergone drastically different thermal histories and have varying properties based on their starting state. Additionally it was shown that these initial variations can result in preferential densification "paths", along which high current will pass and sinter material locally. Depending on processing parameters and sintering times, this can result in compacts with heterogeneous microstructures, significant transient stresses, and final distortion. Such phenomena are expected to be exaggerated in complex shape parts and need to be taken into account during design and optimization of electric current sintering operations.

Acknowledgements Partial financial support from grants NSF-DMI-0400168 and DAAD19-03-2-0023 (ARO/ARL) is acknowledged. BM would like to acknowledge financial support from DoEd GAANN program P200A060117.

References

1. Groza JR, Zavaliangos A (2000) Sintering activation by external electrical field. Mater Sci Eng A 287(2):171–177. doi:10.1016/S0921-5093(00)00771-1
2. Zhang J (2004) Numerical simulation of transient thermoelectric phenomena in field activated sintering. Drexel University, Philadelphia, PA
3. Vanmeensel K et al (2007) Field assisted sintering of electro-conductive ZrO2-based composites. J Eur Ceram Soc 27(2–3): 979–985. doi:10.1016/j.jeurceramsoc.2006.04.142

4. Zavaliangos A et al (2004) Temperature evolution during field activated sintering. Mater Sci Eng A 379
5. McWilliams B, Zavaliangos A (2004) Towards the design and optimization of sintering aided by electric current for high melting point materials. In: International conference on powder metallurgy and particulate materials, Chicago, IL
6. Vanmeensel K et al (2005) Modeling of the temperature distribution during field assisted sintering. Acta Mater 53:4379. doi:10.1016/j.actamat.2005.05.042
7. McWilliams B et al (2006) The modeling of electric-current-assisted sintering to produce bulk nanocrystalline tungsten. JOM 58(4):67. doi:10.1007/s11837-006-0218-2
8. McWilliams B, Zavaliangos A (2007) Multi-phenomena simulation of electric field assisted sintering. In: International conference on powder metallurgy & particulate materials, Denver, CO
9. Gillia O, Bouvard D (2000) Phenomenological analysis of densification kinetics during sintering: application to WC–Co mixture. Mater Sci Eng A 279:185–191. doi:10.1016/S0921-5093(99)00621-8
10. Kim H et al (2002) Near net shape processing of a sintered alumina component: adjustment of pressing parameters through finite element simulation. Int J Mech Sci 44:2523–2539. doi:10.1016/S0020-7403(02)00189-3
11. Raichenko AI (1987) Fundamental processes in powder sintering. Metalurgiya, Moscow